

FOCUSING WAVES THROUGH A RANDOMLY SCATTERING MEDIUM IN THE WHITE-NOISE PARAXIAL REGIME*

JOSSELIN GARNIER[†] AND KNUT SØLNA[‡]

Abstract. When waves propagate through a complex or heterogeneous medium the wave field is corrupted by the heterogeneities. Such corruption limits the performance of imaging or communication schemes. One may then ask the question, Is there an optimal way of encoding a signal so as to counteract the corruption by the medium? In the ideal situation the answer is given by time reversal: for a given target or focusing point, in a first step let the target emit a signal and then record the signal transmitted to the source antenna, time reverse this, and use it as the source trace at the source antenna in a second step. This source will give a sharply focused wave at the target location if the source aperture is large enough. Here we address this scheme in the more practical situation with a limited aperture, time-harmonic signal, and finite-sized elements in the source array. Central questions are then the focusing resolution and signal-to-noise ratio at the target, their dependence on the physical parameters, and the capacity to focus selectively in the neighborhood of the target point and therefore to transmit images. Sharp results are presented for these questions.

Key words. waves in random media, multiple scattering, parabolic approximation, time reversal

AMS subject classifications. 60H15, 35R60, 74J20

DOI. 10.1137/16M1087266

1. Introduction. Wavefront-shaping-based schemes for focusing [19, 23, 24, 25] and imaging [20, 17, 15] have proved very useful for focusing and imaging through scattering media. The primary goal of the experiments reported in these papers is to focus monochromatic light through a layer of strongly scattering material. This is a challenging problem as it is known that multiple scattering of waves by the medium inhomogeneities scrambles the transmitted light into random interference patterns called speckle patterns [13]. However, if a spatial light modulator (SLM) is applied before the scattering medium, then it is possible to focus light as first demonstrated in [24]. Indeed, the elements of the SLM can impose phase shifts prescribed by the user, and it is possible to choose (by an optimization scheme) the phase shifts so as to maximize the intensity transmitted at one point in the target plane behind the scattering medium (see Figure 1).

It turns out that the phase shifts obtained by the wavefront-shaping optimization procedure are the opposite phases of the field emitted by a point source at the target point and recorded in the plane of the SLM [17]. In other words, the wavefront-shaping optimization procedure is equivalent to phase conjugation or time reversal. The focal spot obtained at the target point by the wavefront-shaping-based scheme is the focal spot of the time-reversed refocused wave obtained at the end of a time-reversal experiment in which waves emitted by a source at the target point propagate through the scattering medium, are recorded by an array of sensors in the plane of the

*Received by the editors August 1, 2016; accepted for publication (in revised form) December 29, 2016; published electronically March 30, 2017.

<http://www.siam.org/journals/siap/77-2/M108726.html>

Funding: This work was partly supported by AFOSR grant FA9550-11-1-0176 and ANR project SURMITO.

[†]Laboratoire de Probabilités et Modèles Aléatoires and Laboratoire Jacques-Louis Lions, Université Paris Diderot, 75205 Paris Cedex 13, France (garnier@math.univ-paris-diderot.fr).

[‡]Department of Mathematics, University of California, Irvine, CA 92697 (ksolna@math.uci.edu).

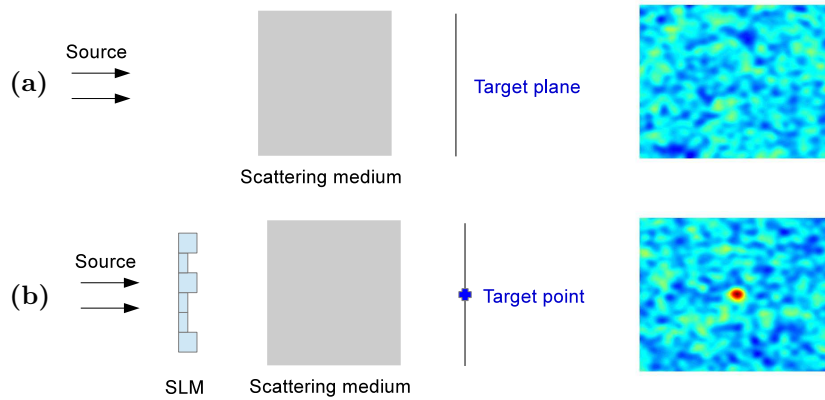


FIG. 1. *Focusing wave through a scattering medium. Without any control one gets a speckle pattern (shown in the right picture) in the target plane (a). With an SLM one can focus on a target point by imposing appropriate phase shifts (b).*

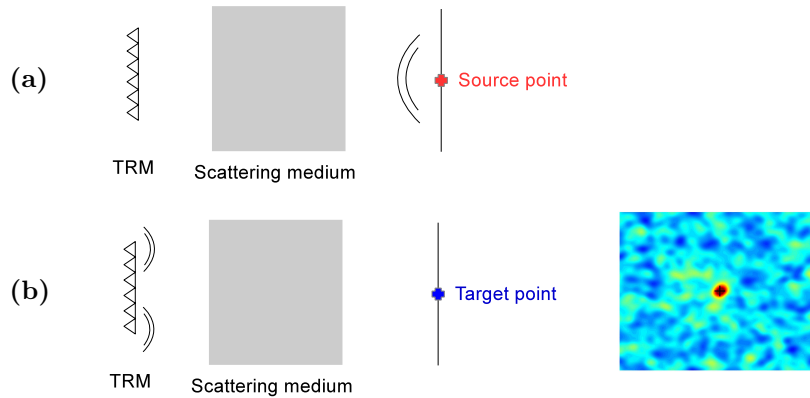


FIG. 2. *Time-reversal experiment through a scattering medium. In the first step of the experiment (a) a time-harmonic point source emits a wave that propagates through the scattering medium and is recorded by the time-reversal mirror (TRM) used as an array of receivers. In the second step of the experiment (b) the TRM is used as an array of sources, it emits the complex-conjugated (i.e., time-reversed) recorded field, and the wave refocuses at the original source location. The right picture is the transmitted field in the target plane, that is, the original source plane. The cross in the right picture is the original source location. One can see that the transmitted field has a focal spot that is centered at the cross.*

SLM, are time-reversed, and are reemitted through the scattering medium toward the plane of the target (see Figure 2). This time-reversal interpretation and the known refocusing and stability properties of time reversal for waves in random media [16, 5] explain the focusing properties of the wavefront-shaping-based scheme [17].

However, two questions can be raised in view of the experimental results:

- The elements of the SLM are much larger than the operating wavelength (for instance, $20\mu\text{m}$ for the SLM used in [24, 25]) and may even be larger than the correlation radius of a field emitted from the target point and transmitted through the scattering medium. This means that the phase shifts imposed by the elements of the SLM are not the phases of the conjugated (or

time-reversed) field but result from local averages of this field. Nevertheless refocusing seems very efficient. We will see that indeed time reversal with a smoothing kernel whose radius is larger than the correlation radius allows for wave refocusing, that the radius of the focal spot at the target point does not depend on the smoothing, but that the statistical stability of the focal spot (i.e., the signal-to-noise ratio) depends on it.

- The SLM is used to correct the wavefront distortions of the diffused light. After performing the correction for a target point, it turns out that the correction can also be used to make the wave focus on a prescribed neighboring point, which allows for transmitting images. This is explained in the physical literature by the memory effect for speckle correlations [4, 7, 15]. We will see that indeed it is possible to focus selectively at any point in a neighborhood of the target point, which allows us to transmit an image, and we will quantify the extent of this neighborhood and the resolution and the stability of the image obtained by this method.

We address in this paper these questions in the paraxial white-noise regime, as described by the Itô–Schrödinger model for the Green’s function. This model is a simplification of the Helmholtz equation with random index of refraction; it gives the correct statistical structure of the wave field when the propagation distance is larger than the correlation length of the medium which is itself larger than the wavelength and when the typical amplitude of the medium fluctuations is small. The Itô–Schrödinger model can be derived rigorously from the Helmholtz equation by a separation of scales technique in the high-frequency regime [8, 9, 10]. It is physically relevant and it models many situations, for instance, laser beam propagation [1, 21], time reversal in random media [2, 18], or underwater acoustics [22]. The Itô–Schrödinger model allows for the use of Itô’s stochastic calculus, which in turn enables the closure of the hierarchy of moment equations [6, 14]. Until recently, the equation for the fourth-order moments of the Green’s function could not be solved [14, sect. 20.18]. However, in a recent paper [12] (with a preliminary version in [11]) the behavior of the fourth-order moments of the random paraxial Green’s function could be unraveled and our paper is based on this result that allows us to carry out a variance analysis of the time-reversed field (which indeed involves fourth-order moments of the Green’s function).

The paper is organized as follows. We describe the transmission problem in section 2. In section 3 we extend the result obtained in [12] in order to get the fourth-order moment that is of interest for our study. In section 4 we prove Propositions 4.1 and 4.2 that describe the mean and covariance of the refocused field around the target point. In section 5 we show how to focus on a prescribed point in the neighborhood of the target point and use this idea in section 6 to show that it possible to transmit an image through a strongly scattering medium.

2. Time-reversal experiment. In this paper we denote the three-dimensional spatial variable by (\mathbf{x}, z) with $\mathbf{x} \in \mathbb{R}^2$ the transverse variable and $z \in \mathbb{R}$ the longitudinal variable. A time-reversal mirror (TRM) is located in the plane $z = 0$. Its radius is R_m and the radius of its elements is ρ_0 .

In the first step of the time-reversal experiment, a point source localized at (\mathbf{y}, L) emits a time-harmonic signal at frequency ω . The TRM is used as an array of receivers and records the wave emitted by the point source. The size ρ_0 of the elements of the TRM is taken into account in the form of a Gaussian smoothing kernel with radius ρ_0 . By denoting $\hat{\mathcal{G}}(L, \mathbf{x}_m, \mathbf{y})$ the Green’s function from $(\mathbf{x}_m, 0)$ to (\mathbf{y}, L) (which is equal

to the Green's function from (\mathbf{y}, L) to $(\mathbf{x}_m, 0)$ by reciprocity), the recorded field at $(\mathbf{x}_m, 0)$ is therefore obtained via the smoothing over the Gaussian mirror element as

$$(2.1) \quad \hat{u}_{\text{rec}}(\mathbf{x}_m; \mathbf{y}) = \frac{1}{2\pi\rho_0^2} \int \hat{G}(L, \mathbf{x}_m + \mathbf{x}', \mathbf{y}) \exp\left(-\frac{|\mathbf{x}'|^2}{2\rho_0^2}\right) d\mathbf{x}'.$$

In the second step of the time-reversal experiment, the TRM is used as an array of sources. It emits the time-reversed (or complex-conjugated) recorded field $\overline{\hat{u}_{\text{rec}}}$. The time-reversed field observed in the plane $z = L$ at the point (\mathbf{x}, L) has the form

$$(2.2) \quad \hat{u}_{\text{tr}}(\mathbf{x}; \mathbf{y}) = \int \hat{u}_{\text{em}}(\mathbf{x}, \mathbf{x}_m) \exp\left(-\frac{|\mathbf{x}_m|^2}{R_m^2}\right) \overline{\hat{u}_{\text{rec}}(\mathbf{x}_m; \mathbf{y})} d\mathbf{x}_m.$$

Here we have assumed that the TRM has a radius R_m and can be modeled by a Gaussian spatial cut-off function. Moreover, we again take into account the size ρ_0 of the elements of the TRM by considering that from any point $(\mathbf{x}_m, 0)$ the TRM can emit from a patch with radius ρ_0 and with a Gaussian form, which generates the following field at point (\mathbf{x}, L) :

$$(2.3) \quad \hat{u}_{\text{em}}(\mathbf{x}; \mathbf{x}_m) = \frac{1}{2\pi\rho_0^2} \int \hat{G}(L, \mathbf{x}_m + \mathbf{x}', \mathbf{x}) \exp\left(-\frac{|\mathbf{x}'|^2}{2\rho_0^2}\right) d\mathbf{x}'.$$

The time-reversed field observed in the plane $z = L$ can therefore be expressed as

$$(2.4) \quad \hat{u}_{\text{tr}}(\mathbf{x}; \mathbf{y}) = 4k_0^2 C_0 \iint \exp\left(-\frac{|\mathbf{x}'|^2}{r_0^2} - \frac{|\mathbf{y}'|^2}{4\rho_0^2}\right) \hat{G}\left(L, \mathbf{x}' + \frac{\mathbf{y}'}{2}, \mathbf{x}\right) \overline{\hat{G}\left(L, \mathbf{x}' - \frac{\mathbf{y}'}{2}, \mathbf{y}\right)} d\mathbf{x}' d\mathbf{y}'$$

with

$$(2.5) \quad C_0 = \frac{r_0^2 - \rho_0^2}{16\pi k_0^2 \rho_0^2 r_0^2}, \quad r_0^2 = R_m^2 + \rho_0^2.$$

Of course, when the size of the elements ρ_0 goes to zero, we recover the standard expression for the refocused time-reversed field with a TRM with a Gaussian aperture with radius R_m :

$$\hat{u}_{\text{tr}}(\mathbf{x}; \mathbf{y})|_{\rho \rightarrow 0} = \int \exp\left(-\frac{|\mathbf{x}'|^2}{R_m^2}\right) \hat{G}(L, \mathbf{x}', \mathbf{x}) \overline{\hat{G}(L, \mathbf{x}', \mathbf{y})} d\mathbf{x}'.$$

From now on we will take $C_0 = 1$ as this multiplicative factor does not play any role in what follows.

Remark 2.1. We have modeled the global shape of the TRM and the local shape of the elements of the TRM by soft Gaussian cut-off functions, instead of hard cut-off functions such as $\mathbf{1}_{[0, R_m]}(|\mathbf{x}_m|)$ or $\mathbf{1}_{[0, \rho_0]}(|\mathbf{x}'|)$, because this allows us to get simple and explicit expressions in the following.

2.1. The Green's function in the white-noise paraxial regime. In the white-noise paraxial regime the Green's function \hat{G} is of the form [12]

$$\hat{G}(L, \mathbf{x}, \mathbf{y}) = \frac{i}{2k_0} e^{ik_0 L} \hat{G}(L, \mathbf{x}, \mathbf{y}),$$

where k_0 is the homogeneous wavenumber and the function \hat{G} is the solution of the Itô-Schrödinger equation

$$(2.6) \quad d\hat{G}(z, \mathbf{x}, \mathbf{y}) = \frac{i}{2k_0} \Delta_{\mathbf{x}} \hat{G}(z, \mathbf{x}, \mathbf{y}) dz + \frac{ik_0}{2} \hat{G}(z, \mathbf{x}, \mathbf{y}) \circ dB(z, \mathbf{x})$$

with the initial condition in the plane $z = 0$: $\hat{G}(z = 0, \mathbf{x}, \mathbf{y}) = \delta(\mathbf{x} - \mathbf{y})$. Here the symbol \circ stands for the Stratonovich stochastic integral, $B(z, \mathbf{x})$ is a real-valued Brownian field over $[0, \infty) \times \mathbb{R}^2$ with covariance

$$(2.7) \quad \mathbb{E}[B(z, \mathbf{x})B(z', \mathbf{x}')] = \min\{z, z'\}C(\mathbf{x} - \mathbf{x}'),$$

and C is determined by the two-point statistics of the fluctuations of the random medium (in particular the width of C is the correlation length of the medium fluctuations). In Itô's form (2.6) reads

$$(2.8) \quad d\hat{G}(z, \mathbf{x}, \mathbf{y}) = \frac{i}{2k_0}\Delta_{\mathbf{x}}\hat{G}(z, \mathbf{x}, \mathbf{y})dz + \frac{ik_0}{2}\hat{G}(z, \mathbf{x}, \mathbf{y})dB(z, \mathbf{x}) - \frac{k_0^2}{8}C(\mathbf{0})\hat{G}(z, \mathbf{x}, \mathbf{y})dz.$$

This equation was analyzed for the first time in [3] and it was derived from first principles by a multiscale analysis of the wave equation in a random medium in [9]. In Appendix A we further discuss this model and the scintillation regime that we introduce below in section 3. Note that in the white-noise paraxial regime, the time-reversed field is

$$(2.9) \quad \hat{u}_{\text{tr}}(\mathbf{x}; \mathbf{y}) = \iint \exp\left(-\frac{|\mathbf{x}'|^2}{r_0^2} - \frac{|\mathbf{y}'|^2}{4\rho_0^2}\right) \hat{G}\left(L, \mathbf{x}' + \frac{\mathbf{y}'}{2}, \mathbf{x}\right) \overline{\hat{G}\left(L, \mathbf{x}' - \frac{\mathbf{y}'}{2}, \mathbf{y}\right)} d\mathbf{x}' d\mathbf{y}'.$$

In the white-noise paraxial regime one can derive transport equations for the moments of the wave field. These moments are important since they allow us to characterize the time-reversed and refocused field. The two first moments can be computed explicitly; however, for the fourth moment there is no explicit expression in the general case. A novel aspect of our analysis is that we here get an explicit characterization of the fourth moment of the wave field in the scintillation regime introduced in section 3. This is important since it allows us to compute a signal-to-noise ratio for the refocused field. Next we characterize respectively the mean refocused wave and also its signal-to-noise ratio that characterizes its relative fluctuations.

2.2. The mean refocused wave. The mean time-reversed field observed at (\mathbf{x}, L) when the original source is at (\mathbf{y}, L) is

$$(2.10) \quad M_1(L, \mathbf{x}, \mathbf{y}) = \mathbb{E}[\hat{u}_{\text{tr}}(\mathbf{x}; \mathbf{y})],$$

and it can be expressed as

$$M_1(L, \mathbf{x}, \mathbf{y}) = \iint \exp\left(-\frac{|\mathbf{x}'|^2}{r_0^2} - \frac{|\mathbf{y}'|^2}{4\rho_0^2}\right) \mathbb{E}\left[\hat{G}\left(L, \mathbf{x}' + \frac{\mathbf{y}'}{2}, \mathbf{x}\right) \overline{\hat{G}\left(L, \mathbf{x}' - \frac{\mathbf{y}'}{2}, \mathbf{y}\right)}\right] d\mathbf{x}' d\mathbf{y}'.$$

M_1 satisfies the system

$$(2.11) \quad \frac{\partial M_1}{\partial z} = \frac{i}{2k_0}(\Delta_{\mathbf{x}} - \Delta_{\mathbf{y}})M_1 + \frac{k_0^2}{4}(C(\mathbf{x} - \mathbf{y}) - C(\mathbf{0}))M_1,$$

starting from

$$M_1(z = 0, \mathbf{x}, \mathbf{y}) = \exp\left(-\frac{|\mathbf{x} + \mathbf{y}|^2}{4r_0^2} - \frac{|\mathbf{x} - \mathbf{y}|^2}{4\rho_0^2}\right).$$

After parameterizing the two points \mathbf{x} and \mathbf{y} as

$$\mathbf{r} = \frac{\mathbf{x} + \mathbf{y}}{2}, \quad \mathbf{q} = \mathbf{x} - \mathbf{y},$$

this equation can be solved (after Fourier transforming in \mathbf{r}):

$$(2.12) \quad M_1 \left(L, \mathbf{r} + \frac{\mathbf{q}}{2}, \mathbf{r} - \frac{\mathbf{q}}{2} \right) = \frac{r_0^2}{4\pi} \int \exp \left(i\boldsymbol{\xi} \cdot \mathbf{r} - \frac{r_0^2 |\boldsymbol{\xi}|^2}{4} - \frac{|\mathbf{q} - \boldsymbol{\xi} \frac{L}{k_0}|^2}{4\rho_0^2} + \frac{k_0^2}{4} \int_0^L C \left(\mathbf{q} - \boldsymbol{\xi} \frac{z}{k_0} \right) - C(\mathbf{0}) dz \right) d\boldsymbol{\xi}.$$

2.3. The fluctuations of the refocused wave. We consider the general second-order moment for the time-reversed wave

$$(2.13) \quad \begin{aligned} M_2(L, \mathbf{x}_1, \mathbf{x}_2, \mathbf{y}_1, \mathbf{y}_2) &= \mathbb{E} [\hat{u}_{\text{tr}}(\mathbf{x}_1; \mathbf{y}_1) \overline{\hat{u}_{\text{tr}}(\mathbf{x}_2; \mathbf{y}_2)}] \\ &= \mathbb{E} [\hat{u}_{\text{tr}}(\mathbf{x}_1; \mathbf{y}_1) \hat{u}_{\text{tr}}(\mathbf{x}_2; \mathbf{y}_2)], \end{aligned}$$

which depends on the fourth-order moment of the paraxial Green's function:

$$\begin{aligned} M_2(L, \mathbf{x}_1, \mathbf{x}_2, \mathbf{y}_1, \mathbf{y}_2) &= \iint \exp \left(-\frac{|\mathbf{x}'_1|^2 + |\mathbf{x}'_2|^2}{r_0^2} - \frac{|\mathbf{y}'_1|^2 + |\mathbf{y}'_2|^2}{4\rho_0^2} \right) \\ &\quad \times \mathbb{E} \left[\hat{G} \left(L, \mathbf{x}'_1 + \frac{\mathbf{y}'_1}{2}, \mathbf{x}_1 \right) \hat{G} \left(L, \mathbf{x}'_2 + \frac{\mathbf{y}'_2}{2}, \mathbf{x}_2 \right) \right. \\ &\quad \left. \times \overline{\hat{G} \left(L, \mathbf{x}'_1 - \frac{\mathbf{y}'_1}{2}, \mathbf{y}_1 \right) \hat{G} \left(L, \mathbf{x}'_2 - \frac{\mathbf{y}'_2}{2}, \mathbf{y}_2 \right)} \right] d\mathbf{x}'_1 d\mathbf{y}'_1 d\mathbf{x}'_2 d\mathbf{y}'_2. \end{aligned}$$

It satisfies

$$(2.14) \quad \frac{\partial M_2}{\partial z} = \frac{i}{2k_0} (\Delta_{\mathbf{x}_1} + \Delta_{\mathbf{x}_2} - \Delta_{\mathbf{y}_1} - \Delta_{\mathbf{y}_2}) M_2 + \frac{k_0^2}{4} U_2(\mathbf{x}_1, \mathbf{x}_2, \mathbf{y}_1, \mathbf{y}_2) M_2,$$

with the generalized potential

$$(2.15) \quad \begin{aligned} U_2(\mathbf{x}_1, \mathbf{x}_2, \mathbf{y}_1, \mathbf{y}_2) &= C(\mathbf{x}_1 - \mathbf{y}_1) + C(\mathbf{x}_1 - \mathbf{y}_2) + C(\mathbf{x}_2 - \mathbf{y}_1) + C(\mathbf{x}_2 - \mathbf{y}_2) \\ &\quad - C(\mathbf{x}_1 - \mathbf{x}_2) - C(\mathbf{y}_1 - \mathbf{y}_2) - 2C(\mathbf{0}), \end{aligned}$$

and it starts from

$$\begin{aligned} M_2(z = 0, \mathbf{x}_1, \mathbf{x}_2, \mathbf{y}_1, \mathbf{y}_2) &= \exp \left(-\frac{|\mathbf{x}_1 + \mathbf{y}_1|^2 + |\mathbf{x}_2 + \mathbf{y}_2|^2}{4r_0^2} \right) \\ &\quad \times \exp \left(-\frac{|\mathbf{x}_1 - \mathbf{y}_1|^2 + |\mathbf{x}_2 - \mathbf{y}_2|^2}{4\rho_0^2} \right). \end{aligned}$$

We parameterize the four points $\mathbf{x}_1, \mathbf{x}_2, \mathbf{y}_1, \mathbf{y}_2$ in (2.14) in the special way:

$$\begin{aligned} \mathbf{x}_1 &= \frac{\mathbf{r}_1 + \mathbf{r}_2 + \mathbf{q}_1 + \mathbf{q}_2}{2}, & \mathbf{y}_1 &= \frac{\mathbf{r}_1 + \mathbf{r}_2 - \mathbf{q}_1 - \mathbf{q}_2}{2}, \\ \mathbf{x}_2 &= \frac{\mathbf{r}_1 - \mathbf{r}_2 + \mathbf{q}_1 - \mathbf{q}_2}{2}, & \mathbf{y}_2 &= \frac{\mathbf{r}_1 - \mathbf{r}_2 - \mathbf{q}_1 + \mathbf{q}_2}{2}. \end{aligned}$$

In particular $\mathbf{r}_1/2$ is the barycenter of the four points $\mathbf{x}_1, \mathbf{x}_2, \mathbf{y}_1, \mathbf{y}_2$:

$$\begin{aligned} \mathbf{r}_1 &= \frac{\mathbf{x}_1 + \mathbf{x}_2 + \mathbf{y}_1 + \mathbf{y}_2}{2}, & \mathbf{q}_1 &= \frac{\mathbf{x}_1 + \mathbf{x}_2 - \mathbf{y}_1 - \mathbf{y}_2}{2}, \\ \mathbf{r}_2 &= \frac{\mathbf{x}_1 - \mathbf{x}_2 + \mathbf{y}_1 - \mathbf{y}_2}{2}, & \mathbf{q}_2 &= \frac{\mathbf{x}_1 - \mathbf{x}_2 - \mathbf{y}_1 + \mathbf{y}_2}{2}. \end{aligned}$$

In the variables $(\mathbf{q}_1, \mathbf{q}_2, \mathbf{r}_1, \mathbf{r}_2)$ the function M_2 satisfies the equation

$$(2.16) \quad \frac{\partial M_2}{\partial z} = \frac{i}{k_0} (\nabla_{\mathbf{r}_1} \cdot \nabla_{\mathbf{q}_1} + \nabla_{\mathbf{r}_2} \cdot \nabla_{\mathbf{q}_2}) M_2 + \frac{k_0^2}{4} U_2(\mathbf{q}_1, \mathbf{q}_2, \mathbf{r}_1, \mathbf{r}_2) M_2,$$

with the generalized potential

$$(2.17) \quad \begin{aligned} U_2(\mathbf{q}_1, \mathbf{q}_2, \mathbf{r}_1, \mathbf{r}_2) &= C(\mathbf{q}_2 + \mathbf{q}_1) + C(\mathbf{q}_2 - \mathbf{q}_1) + C(\mathbf{r}_2 + \mathbf{q}_1) + C(\mathbf{r}_2 - \mathbf{q}_1) \\ &\quad - C(\mathbf{q}_2 + \mathbf{r}_2) - C(\mathbf{q}_2 - \mathbf{r}_2) - 2C(\mathbf{0}). \end{aligned}$$

Note in particular that the generalized potential does not depend on the barycenter \mathbf{r}_1 as the medium is statistically homogeneous. The initial condition for (2.16) is

$$M_2(z = 0, \mathbf{q}_1, \mathbf{q}_2, \mathbf{r}_1, \mathbf{r}_2) = \exp\left(-\frac{|\mathbf{r}_1|^2 + |\mathbf{r}_2|^2}{2r_0^2} - \frac{|\mathbf{q}_1|^2 + |\mathbf{q}_2|^2}{2\rho_0^2}\right).$$

The second moment of the refocused wave field can be expressed as

$$(2.18) \quad \mathbb{E}[\hat{u}_{\text{tr}}(\mathbf{x}, \mathbf{y})^2] = M_2(L, \mathbf{r}_1 = \mathbf{x} + \mathbf{y}, \mathbf{r}_2 = \mathbf{0}, \mathbf{q}_1 = \mathbf{0}, \mathbf{q}_2 = \mathbf{x} - \mathbf{y}),$$

and, more generally,

$$(2.19) \quad \mathbb{E}\left[\hat{u}_{\text{tr}}\left(\mathbf{x} + \frac{\mathbf{h}}{2}, \mathbf{y}\right) \overline{\hat{u}_{\text{tr}}\left(\mathbf{x} - \frac{\mathbf{h}}{2}, \mathbf{y}\right)}\right] = M_2\left(L, \mathbf{r}_1 = \mathbf{x} + \mathbf{y}, \mathbf{r}_2 = \frac{\mathbf{h}}{2}, \mathbf{q}_1 = \frac{\mathbf{h}}{2}, \mathbf{q}_2 = \mathbf{x} - \mathbf{y}\right).$$

The Fourier transform (in $\mathbf{q}_1, \mathbf{q}_2, \mathbf{r}_1,$ and \mathbf{r}_2) of the fourth-order moment of the paraxial Green's function is defined by

$$(2.20) \quad \begin{aligned} \hat{M}_2(z, \boldsymbol{\xi}_1, \boldsymbol{\xi}_2, \boldsymbol{\zeta}_1, \boldsymbol{\zeta}_2) &= \iint M_2(z, \mathbf{q}_1, \mathbf{q}_2, \mathbf{r}_1, \mathbf{r}_2) \\ &\quad \times \exp(-i\mathbf{q}_1 \cdot \boldsymbol{\xi}_1 - i\mathbf{r}_1 \cdot \boldsymbol{\zeta}_1 - i\mathbf{q}_2 \cdot \boldsymbol{\xi}_2 - i\mathbf{r}_2 \cdot \boldsymbol{\zeta}_2) d\mathbf{r}_1 d\mathbf{r}_2 d\mathbf{q}_1 d\mathbf{q}_2. \end{aligned}$$

It satisfies

$$(2.21) \quad \begin{aligned} \frac{\partial \hat{M}_2}{\partial z} + \frac{i}{k_0} (\boldsymbol{\xi}_1 \cdot \boldsymbol{\zeta}_1 + \boldsymbol{\xi}_2 \cdot \boldsymbol{\zeta}_2) \hat{M}_2 &= \frac{k_0^2}{4(2\pi)^2} \int \hat{C}(\mathbf{k}) \left[\hat{M}_2(\boldsymbol{\xi}_1 - \mathbf{k}, \boldsymbol{\xi}_2 - \mathbf{k}, \boldsymbol{\zeta}_1, \boldsymbol{\zeta}_2) \right. \\ &\quad + \hat{M}_2(\boldsymbol{\xi}_1 - \mathbf{k}, \boldsymbol{\xi}_2, \boldsymbol{\zeta}_1, \boldsymbol{\zeta}_2 - \mathbf{k}) + \hat{M}_2(\boldsymbol{\xi}_1 + \mathbf{k}, \boldsymbol{\xi}_2 - \mathbf{k}, \boldsymbol{\zeta}_1, \boldsymbol{\zeta}_2) \\ &\quad + \hat{M}_2(\boldsymbol{\xi}_1 + \mathbf{k}, \boldsymbol{\xi}_2, \boldsymbol{\zeta}_1, \boldsymbol{\zeta}_2 - \mathbf{k}) - 2\hat{M}_2(\boldsymbol{\xi}_1, \boldsymbol{\xi}_2, \boldsymbol{\zeta}_1, \boldsymbol{\zeta}_2) \\ &\quad \left. - \hat{M}_2(\boldsymbol{\xi}_1, \boldsymbol{\xi}_2 - \mathbf{k}, \boldsymbol{\zeta}_1, \boldsymbol{\zeta}_2 - \mathbf{k}) - \hat{M}_2(\boldsymbol{\xi}_1, \boldsymbol{\xi}_2 + \mathbf{k}, \boldsymbol{\zeta}_1, \boldsymbol{\zeta}_2 - \mathbf{k}) \right] d\mathbf{k}, \end{aligned}$$

starting from

$$\hat{M}_2(z = 0, \boldsymbol{\xi}_1, \boldsymbol{\xi}_2, \boldsymbol{\zeta}_1, \boldsymbol{\zeta}_2) = (2\pi r_0 \rho_0)^4 \exp\left(-\frac{\rho_0^2}{2} (|\boldsymbol{\xi}_1|^2 + |\boldsymbol{\xi}_2|^2) - \frac{r_0^2}{2} (|\boldsymbol{\zeta}_1|^2 + |\boldsymbol{\zeta}_2|^2)\right).$$

The solution of this transport equation would give the expression of the variance of the refocused wave. However, in contrast to the second-order moment of the paraxial Green's function, we cannot solve this equation and find a closed-form expression. Therefore we address in the next sections a particular regime in which explicit expressions can be obtained.

3. The scintillation regime. In this paper we address a regime which can be considered as a particular case of the paraxial white-noise regime: the scintillation regime. The scintillation regime is valid if the transverse correlation length of the Brownian field B (which is the correlation length of the medium) is smaller than the radius of the TRM and the one of the smoothing kernel. If the correlation length is our reference length, this means that in this regime the covariance function C^ε , the radius of the TRM r_0^ε , the smoothing kernel radius ρ_0^ε , and the propagation distance L^ε are of the form

$$(3.1) \quad C^\varepsilon(\mathbf{x}) = \varepsilon C(\mathbf{x}), \quad r_0^\varepsilon = \frac{r_0}{\varepsilon}, \quad \rho_0^\varepsilon = \frac{\rho_0}{\varepsilon}, \quad L^\varepsilon = \frac{L}{\varepsilon}.$$

Here ε is a small dimensionless parameter and we will study the limit $\varepsilon \rightarrow 0$. We discuss further the scintillation regime in Appendix A. Assuming the scintillation regime let us introduce the rescaled function

$$(3.2) \quad \widetilde{M}^\varepsilon(z, \boldsymbol{\xi}_1, \boldsymbol{\xi}_2, \boldsymbol{\zeta}_1, \boldsymbol{\zeta}_2) = \widehat{M}_2^\varepsilon\left(\frac{z}{\varepsilon}, \boldsymbol{\xi}_1, \boldsymbol{\xi}_2, \boldsymbol{\zeta}_1, \boldsymbol{\zeta}_2\right) \exp\left(\frac{iz}{k_0\varepsilon}(\boldsymbol{\xi}_2 \cdot \boldsymbol{\zeta}_2 + \boldsymbol{\xi}_1 \cdot \boldsymbol{\zeta}_1)\right).$$

In the scintillation regime the rescaled function $\widetilde{M}^\varepsilon$ satisfies the equation with fast phases

$$(3.3) \quad \begin{aligned} \frac{\partial \widetilde{M}^\varepsilon}{\partial z} = & \frac{k_0^2}{4(2\pi)^2} \int \widehat{C}(\mathbf{k}) \left[-2\widetilde{M}^\varepsilon(\boldsymbol{\xi}_1, \boldsymbol{\xi}_2, \boldsymbol{\zeta}_1, \boldsymbol{\zeta}_2) \right. \\ & + \widetilde{M}^\varepsilon(\boldsymbol{\xi}_1 - \mathbf{k}, \boldsymbol{\xi}_2 - \mathbf{k}, \boldsymbol{\zeta}_1, \boldsymbol{\zeta}_2) e^{i\frac{z}{\varepsilon k_0} \mathbf{k} \cdot (\boldsymbol{\zeta}_2 + \boldsymbol{\zeta}_1)} \\ & + \widetilde{M}^\varepsilon(\boldsymbol{\xi}_1 - \mathbf{k}, \boldsymbol{\xi}_2, \boldsymbol{\zeta}_1, \boldsymbol{\zeta}_2 - \mathbf{k}) e^{i\frac{z}{\varepsilon k_0} \mathbf{k} \cdot (\boldsymbol{\xi}_2 + \boldsymbol{\zeta}_1)} \\ & + \widetilde{M}^\varepsilon(\boldsymbol{\xi}_1 + \mathbf{k}, \boldsymbol{\xi}_2 - \mathbf{k}, \boldsymbol{\zeta}_1, \boldsymbol{\zeta}_2) e^{i\frac{z}{\varepsilon k_0} \mathbf{k} \cdot (\boldsymbol{\zeta}_2 - \boldsymbol{\zeta}_1)} \\ & + \widetilde{M}^\varepsilon(\boldsymbol{\xi}_1 + \mathbf{k}, \boldsymbol{\xi}_2, \boldsymbol{\zeta}_1, \boldsymbol{\zeta}_2 - \mathbf{k}) e^{i\frac{z}{\varepsilon k_0} \mathbf{k} \cdot (\boldsymbol{\xi}_2 - \boldsymbol{\zeta}_1)} \\ & - \widetilde{M}^\varepsilon(\boldsymbol{\xi}_1, \boldsymbol{\xi}_2 - \mathbf{k}, \boldsymbol{\zeta}_1, \boldsymbol{\zeta}_2 - \mathbf{k}) e^{i\frac{z}{\varepsilon k_0} (\mathbf{k} \cdot (\boldsymbol{\zeta}_2 + \boldsymbol{\xi}_2) - |\mathbf{k}|^2)} \\ & \left. - \widetilde{M}^\varepsilon(\boldsymbol{\xi}_1, \boldsymbol{\xi}_2 - \mathbf{k}, \boldsymbol{\zeta}_1, \boldsymbol{\zeta}_2 + \mathbf{k}) e^{i\frac{z}{\varepsilon k_0} (\mathbf{k} \cdot (\boldsymbol{\zeta}_2 - \boldsymbol{\xi}_2) + |\mathbf{k}|^2)} \right] d\mathbf{k}, \end{aligned}$$

starting from

$$(3.4) \quad \widetilde{M}^\varepsilon(z = 0, \boldsymbol{\xi}_1, \boldsymbol{\xi}_2, \boldsymbol{\zeta}_1, \boldsymbol{\zeta}_2) = (2\pi)^8 \phi_{\rho_0}^\varepsilon(\boldsymbol{\xi}_1) \phi_{\rho_0}^\varepsilon(\boldsymbol{\xi}_2) \phi_{r_0}^\varepsilon(\boldsymbol{\zeta}_1) \phi_{r_0}^\varepsilon(\boldsymbol{\zeta}_2),$$

where we have denoted

$$(3.5) \quad \phi_{\rho_0}^\varepsilon(\boldsymbol{\xi}) = \frac{\rho_0^2}{2\pi\varepsilon^2} \exp\left(-\frac{\rho_0^2}{2\varepsilon^2} |\boldsymbol{\xi}|^2\right),$$

and similarly for $\phi_{r_0}^\varepsilon$. Note that $\phi_{\rho_0}^\varepsilon$ belongs to L^1 and has an L^1 -norm equal to one and that it behaves like a Dirac distribution as $\varepsilon \rightarrow 0$. The following result shows that $\widetilde{M}^\varepsilon$ exhibits a multiscale behavior as $\varepsilon \rightarrow 0$, with some components evolving at the scale ε and some components evolving at the scale 1.

PROPOSITION 3.1. *The function $\widetilde{M}^\varepsilon(z, \boldsymbol{\xi}_1, \boldsymbol{\xi}_2, \boldsymbol{\zeta}_1, \boldsymbol{\zeta}_2)$ can be expanded as*

$$\begin{aligned}
\widetilde{M}^\varepsilon(z, \boldsymbol{\xi}_1, \boldsymbol{\xi}_2, \boldsymbol{\zeta}_1, \boldsymbol{\zeta}_2) &= K(z)\phi_{\rho_0}^\varepsilon(\boldsymbol{\xi}_1)\phi_{\rho_0}^\varepsilon(\boldsymbol{\xi}_2)\phi_{r_0}^\varepsilon(\boldsymbol{\zeta}_1)\phi_{r_0}^\varepsilon(\boldsymbol{\zeta}_2) \\
&+ K(z)\phi_{\rho_0}^\varepsilon\left(\frac{\boldsymbol{\xi}_1 - \boldsymbol{\xi}_2}{\sqrt{2}}\right)\phi_{r_0}^\varepsilon(\boldsymbol{\zeta}_1)\phi_{r_0}^\varepsilon(\boldsymbol{\zeta}_2)A\left(z, \frac{\boldsymbol{\xi}_2 + \boldsymbol{\xi}_1}{2}, \frac{\boldsymbol{\zeta}_2 + \boldsymbol{\zeta}_1}{\varepsilon}\right) \\
&+ K(z)\phi_{\rho_0}^\varepsilon\left(\frac{\boldsymbol{\xi}_1 + \boldsymbol{\xi}_2}{\sqrt{2}}\right)\phi_{r_0}^\varepsilon(\boldsymbol{\zeta}_1)\phi_{r_0}^\varepsilon(\boldsymbol{\zeta}_2)A\left(z, \frac{\boldsymbol{\xi}_2 - \boldsymbol{\xi}_1}{2}, \frac{\boldsymbol{\zeta}_2 - \boldsymbol{\zeta}_1}{\varepsilon}\right) \\
&+ K(z)\phi_{R_0}^\varepsilon\left(\frac{\boldsymbol{\xi}_1 - \boldsymbol{\zeta}_2}{\sqrt{2}}\right)\phi_{r_0}^\varepsilon(\boldsymbol{\zeta}_1)\phi_{\rho_0}^\varepsilon(\boldsymbol{\xi}_2)A\left(z, \frac{\boldsymbol{\zeta}_2 + \boldsymbol{\xi}_1}{2}, \frac{\boldsymbol{\xi}_2 + \boldsymbol{\zeta}_1}{\varepsilon}\right) \\
&+ K(z)\phi_{R_0}^\varepsilon\left(\frac{\boldsymbol{\xi}_1 + \boldsymbol{\zeta}_2}{\sqrt{2}}\right)\phi_{r_0}^\varepsilon(\boldsymbol{\zeta}_1)\phi_{\rho_0}^\varepsilon(\boldsymbol{\xi}_2)A\left(z, \frac{\boldsymbol{\zeta}_2 - \boldsymbol{\xi}_1}{2}, \frac{\boldsymbol{\xi}_2 - \boldsymbol{\zeta}_1}{\varepsilon}\right) \\
&+ K(z)\phi_{r_0}^\varepsilon(\boldsymbol{\zeta}_1)\phi_{r_0}^\varepsilon(\boldsymbol{\zeta}_2)A\left(z, \frac{\boldsymbol{\xi}_2 + \boldsymbol{\xi}_1}{2}, \frac{\boldsymbol{\zeta}_2 + \boldsymbol{\zeta}_1}{\varepsilon}\right)A\left(z, \frac{\boldsymbol{\xi}_2 - \boldsymbol{\xi}_1}{2}, \frac{\boldsymbol{\zeta}_2 - \boldsymbol{\zeta}_1}{\varepsilon}\right) \\
&+ K(z)\phi_{r_0}^\varepsilon(\boldsymbol{\zeta}_1)\phi_{\rho_0}^\varepsilon(\boldsymbol{\xi}_2)A\left(z, \frac{\boldsymbol{\zeta}_2 + \boldsymbol{\xi}_1}{2}, \frac{\boldsymbol{\xi}_2 + \boldsymbol{\zeta}_1}{\varepsilon}\right)A\left(z, \frac{\boldsymbol{\zeta}_2 - \boldsymbol{\xi}_1}{2}, \frac{\boldsymbol{\xi}_2 - \boldsymbol{\zeta}_1}{\varepsilon}\right) \\
(3.6) \quad &+ R^\varepsilon(z, \boldsymbol{\xi}_1, \boldsymbol{\xi}_2, \boldsymbol{\zeta}_1, \boldsymbol{\zeta}_2),
\end{aligned}$$

where

$$(3.7) \quad \frac{1}{R_0^2} = \frac{1}{2} \left(\frac{1}{r_0^2} + \frac{1}{\rho_0^2} \right),$$

the functions K and A are defined by

$$(3.8) \quad K(z) = (2\pi)^8 \exp\left(-\frac{k_0^2}{2} C(\mathbf{0})z\right),$$

$$(3.9) \quad A(z, \boldsymbol{\xi}, \boldsymbol{\zeta}) = \frac{1}{2(2\pi)^2} \int \left[\exp\left(\frac{k_0^2}{4} \int_0^z C\left(\mathbf{x} + \frac{\boldsymbol{\zeta}}{k_0} z'\right) dz'\right) - 1 \right] \exp(-i\boldsymbol{\xi} \cdot \mathbf{x}) d\mathbf{x},$$

and the function R^ε satisfies

$$(3.10) \quad \sup_{z \in [0, Z]} \|R^\varepsilon(z, \cdot, \cdot, \cdot, \cdot)\|_{L^1(\mathbb{R}^2 \times \mathbb{R}^2 \times \mathbb{R}^2 \times \mathbb{R}^2)} \xrightarrow{\varepsilon \rightarrow 0} 0$$

for any $Z > 0$.

This result is an extension of Proposition 6.1 in [12] in which the case $r_0 = \rho_0$ is addressed. It shows that if we deal with an integral of $\widetilde{M}^\varepsilon$ against a bounded function, then we can replace $\widetilde{M}^\varepsilon$ by the right-hand side of (3.6) without the R^ε term up to a negligible error when ε is small. This substitution will allow us to get explicit and quantitative results for the refocusing properties of the SLM scheme.

4. Refocusing at the original source location. In the scintillation regime the mean refocused wave is given by (see (2.12) and take $C \rightarrow \varepsilon C$, $r_0 \rightarrow r_0/\varepsilon$, $\rho_0 \rightarrow \rho_0/\varepsilon$, $\mathbf{y} \rightarrow \mathbf{y}/\varepsilon$, $L \rightarrow L/\varepsilon$)

$$\begin{aligned}
 \mathbb{E} \left[\hat{u}_{\text{tr}}^\varepsilon \left(\frac{\mathbf{y}}{\varepsilon} + \mathbf{x}; \frac{\mathbf{y}}{\varepsilon} \right) \right] &= \frac{r_0^2}{4\pi\varepsilon^2} \int \exp \left(i\boldsymbol{\xi} \cdot \left(\frac{\mathbf{y}}{\varepsilon} + \frac{\mathbf{x}}{2} \right) - \frac{r_0^2|\boldsymbol{\xi}|^2}{4\varepsilon^2} - \frac{|\varepsilon\mathbf{x} - \boldsymbol{\xi} \frac{L}{k_0}|^2}{4\rho_0^2} \right. \\
 &\quad \left. + \frac{k_0^2\varepsilon}{4} \int_0^{L/\varepsilon} C \left(\mathbf{x} - \boldsymbol{\xi} \frac{z}{k_0} \right) - C(\mathbf{0}) dz \right) d\boldsymbol{\xi} \\
 &= \frac{r_0^2}{4\pi} \int \exp \left(i\boldsymbol{\xi} \cdot \left(\mathbf{y} + \frac{\varepsilon\mathbf{x}}{2} \right) - \frac{r_0^2|\boldsymbol{\xi}|^2}{4} - \varepsilon^2 \frac{|\mathbf{x} - \boldsymbol{\xi} \frac{L}{k_0}|^2}{4\rho_0^2} \right. \\
 (4.1) \quad &\quad \left. + \frac{k_0^2}{4} \int_0^L C \left(\mathbf{x} - \boldsymbol{\xi} \frac{z}{k_0} \right) - C(\mathbf{0}) dz \right) d\boldsymbol{\xi}.
 \end{aligned}$$

The following result is then straightforward.

PROPOSITION 4.1. *The mean refocused wave converges as $\varepsilon \rightarrow 0$:*

$$(4.2) \quad \mathbb{E} \left[\hat{u}_{\text{tr}}^\varepsilon \left(\frac{\mathbf{y}}{\varepsilon} + \mathbf{x}; \frac{\mathbf{y}}{\varepsilon} \right) \right] \xrightarrow{\varepsilon \rightarrow 0} \frac{r_0^2}{4\pi} \int \exp \left(i\boldsymbol{\xi} \cdot \mathbf{y} - \frac{r_0^2|\boldsymbol{\xi}|^2}{4} + \frac{k_0^2}{4} \int_0^L C \left(\mathbf{x} - \boldsymbol{\xi} \frac{z}{k_0} \right) - C(\mathbf{0}) dz \right) d\boldsymbol{\xi}.$$

We can observe that if the number of elements of the TRM is large, i.e., $\rho_0 \ll R_m$, then $r_0 \simeq R_m$ and the profile of the mean refocused wave does not depend anymore on the number and size of the elements but only depends on the radius of the TRM. The expression (4.2) shows that, as a function of the offset \mathbf{x} , the mean refocused wave has the form of a peak centered at $\mathbf{x} = \mathbf{0}$. This peak has maximal amplitude

$$(4.3) \quad \mathcal{U}_{\mathbf{b},\mathbf{y}} = \lim_{\varepsilon \rightarrow 0} \mathbb{E} \left[\hat{u}_{\text{tr}}^\varepsilon \left(\frac{\mathbf{y}}{\varepsilon}; \frac{\mathbf{y}}{\varepsilon} \right) \right] = \frac{r_0^2}{4\pi} \int \exp \left(i\boldsymbol{\xi} \cdot \mathbf{y} - \frac{r_0^2|\boldsymbol{\xi}|^2}{4} + \frac{k_0^2}{4} \int_0^L C \left(\boldsymbol{\xi} \frac{z}{k_0} \right) - C(\mathbf{0}) dz \right) d\boldsymbol{\xi},$$

and it raises above the constant background

$$(4.4) \quad \mathcal{U}_{\mathbf{p},\mathbf{y}} = \lim_{|\mathbf{x}| \rightarrow \infty} \lim_{\varepsilon \rightarrow 0} \mathbb{E} \left[\hat{u}_{\text{tr}}^\varepsilon \left(\frac{\mathbf{y}}{\varepsilon} + \mathbf{x}; \frac{\mathbf{y}}{\varepsilon} \right) \right] = \exp \left(-\frac{|\mathbf{y}|^2}{r_0^2} - \frac{k_0^2 C(\mathbf{0}) L}{4} \right).$$

By (2.19), in the scintillation regime, the second moment of the refocused wave is

$$\begin{aligned}
 &\mathbb{E} \left[\hat{u}_{\text{tr}}^\varepsilon \left(\frac{\mathbf{y}}{\varepsilon} + \mathbf{x} + \frac{\mathbf{h}}{2}; \frac{\mathbf{y}}{\varepsilon} \right) \overline{\hat{u}_{\text{tr}}^\varepsilon \left(\frac{\mathbf{y}}{\varepsilon} + \mathbf{x} - \frac{\mathbf{h}}{2}; \frac{\mathbf{y}}{\varepsilon} \right)} \right] \\
 &= M_2^\varepsilon \left(\frac{L}{\varepsilon}, \mathbf{r}_1 = \mathbf{x} + \frac{2\mathbf{y}}{\varepsilon}, \mathbf{r}_2 = \frac{\mathbf{h}}{2}, \mathbf{q}_1 = \frac{\mathbf{h}}{2}, \mathbf{q}_2 = \mathbf{x} \right) \\
 &= \frac{1}{(2\pi)^8} \iint \widetilde{M}^\varepsilon(L, \boldsymbol{\xi}_1, \boldsymbol{\xi}_2, \boldsymbol{\zeta}_1, \boldsymbol{\zeta}_2) \exp \left(i \left(\mathbf{x} + \frac{2\mathbf{y}}{\varepsilon} \right) \cdot \boldsymbol{\zeta}_1 + i \frac{\mathbf{h}}{2} \cdot (\boldsymbol{\zeta}_2 + \boldsymbol{\xi}_1) + i\mathbf{x} \cdot \boldsymbol{\xi}_2 \right) \\
 (4.5) \quad &\times \exp \left(-\frac{iL}{k_0\varepsilon} (\boldsymbol{\xi}_2 \cdot \boldsymbol{\zeta}_2 + \boldsymbol{\xi}_1 \cdot \boldsymbol{\zeta}_1) \right) d\boldsymbol{\xi}_1 d\boldsymbol{\xi}_2 d\boldsymbol{\zeta}_1 d\boldsymbol{\zeta}_2.
 \end{aligned}$$

By Proposition 3.1, we find that it converges as $\varepsilon \rightarrow 0$ to

$$\begin{aligned}
& \mathbb{E} \left[\hat{u}_{\text{tr}}^\varepsilon \left(\frac{\mathbf{y}}{\varepsilon} + \mathbf{x} + \frac{\mathbf{h}}{2}; \frac{\mathbf{y}}{\varepsilon} \right) \overline{\hat{u}_{\text{tr}}^\varepsilon \left(\frac{\mathbf{y}}{\varepsilon} + \mathbf{x} - \frac{\mathbf{h}}{2}; \frac{\mathbf{y}}{\varepsilon} \right)} \right] \xrightarrow{\varepsilon \rightarrow 0} \frac{K}{(2\pi)^8} \int \phi_{r_0}^1(\zeta_1) e^{2i\zeta_1 \cdot \mathbf{y}} d\zeta_1 \\
& + \frac{2K}{(2\pi)^8} \iint \phi_{r_0}^1(\zeta_1) \phi_{r_0}^1(\zeta_2) \left[A(\boldsymbol{\xi}_2, \zeta_2 + \zeta_1) e^{2i\zeta_1 \cdot \mathbf{y} - i\frac{L}{k_0}(\zeta_2 + \zeta_1) \cdot \boldsymbol{\xi}_2 + i\boldsymbol{\xi}_2 \cdot (\mathbf{x} + \frac{\mathbf{h}}{2})} \right. \\
& \quad \left. + A(\boldsymbol{\xi}_2, \zeta_2 - \zeta_1) e^{2i\zeta_1 \cdot \mathbf{y} - i\frac{L}{k_0}(\zeta_2 - \zeta_1) \cdot \boldsymbol{\xi}_2 + i\boldsymbol{\xi}_2 \cdot (\mathbf{x} - \frac{\mathbf{h}}{2})} \right] d\zeta_1 d\zeta_2 d\boldsymbol{\xi}_2 \\
& + \frac{2K}{(2\pi)^8} \iint \phi_{r_0}^1(\zeta_1) \phi_{\rho_0}^1(\boldsymbol{\xi}_2) \left[A(\zeta_2, \boldsymbol{\xi}_2 + \zeta_1) e^{2i\zeta_1 \cdot \mathbf{y} - i\frac{L}{k_0}(\boldsymbol{\xi}_2 + \zeta_1) \cdot \zeta_2 + i\zeta_2 \cdot \mathbf{h}} \right. \\
& \quad \left. + A(\zeta_2, \boldsymbol{\xi}_2 - \zeta_1) e^{2i\zeta_1 \cdot \mathbf{y} - i\frac{L}{k_0}(\boldsymbol{\xi}_2 - \zeta_1) \cdot \zeta_2} \right] d\zeta_1 d\zeta_2 d\boldsymbol{\xi}_2 \\
& + \frac{K}{(2\pi)^8} \iint \phi_{r_0}^1(\zeta_1) \phi_{r_0}^1(\zeta_2) A\left(\frac{\boldsymbol{\xi}_2 + \boldsymbol{\xi}_1}{2}, \zeta_2 + \zeta_1\right) A\left(\frac{\boldsymbol{\xi}_2 - \boldsymbol{\xi}_1}{2}, \zeta_2 - \zeta_1\right) \\
& \quad \times e^{2i\zeta_1 \cdot \mathbf{y} + i\boldsymbol{\xi}_2 \cdot \mathbf{x} - i\frac{L}{k_0}(\boldsymbol{\xi}_1 \cdot \zeta_1 + \boldsymbol{\xi}_2 \cdot \zeta_2) + i\boldsymbol{\xi}_1 \cdot \frac{\mathbf{h}}{2}} d\zeta_1 d\zeta_2 d\boldsymbol{\xi}_1 d\boldsymbol{\xi}_2 \\
& + \frac{K}{(2\pi)^8} \iint \phi_{r_0}^1(\zeta_1) \phi_{\rho_0}^1(\boldsymbol{\xi}_2) A\left(\frac{\zeta_2 + \boldsymbol{\xi}_1}{2}, \boldsymbol{\xi}_2 + \zeta_1\right) A\left(\frac{\zeta_2 - \boldsymbol{\xi}_1}{2}, \boldsymbol{\xi}_2 - \zeta_1\right) \\
& \quad \times e^{2i\zeta_1 \cdot \mathbf{y} - i\frac{L}{k_0}(\boldsymbol{\xi}_1 \cdot \zeta_1 + \boldsymbol{\xi}_2 \cdot \zeta_2) + i(\zeta_2 + \boldsymbol{\xi}_1) \cdot \frac{\mathbf{h}}{2}} d\zeta_1 d\zeta_2 d\boldsymbol{\xi}_1 d\boldsymbol{\xi}_2.
\end{aligned} \tag{4.6}$$

Using the explicit expressions (3.8) and (3.9) for K and A , we get

$$\begin{aligned}
& \mathbb{E} \left[\hat{u}_{\text{tr}}^\varepsilon \left(\frac{\mathbf{y}}{\varepsilon} + \mathbf{x} + \frac{\mathbf{h}}{2}; \frac{\mathbf{y}}{\varepsilon} \right) \overline{\hat{u}_{\text{tr}}^\varepsilon \left(\frac{\mathbf{y}}{\varepsilon} + \mathbf{x} - \frac{\mathbf{h}}{2}; \frac{\mathbf{y}}{\varepsilon} \right)} \right] \xrightarrow{\varepsilon \rightarrow 0} -\exp\left(-\frac{k_0^2 C(\mathbf{0})L}{2} - \frac{2|\mathbf{y}|^2}{r_0^2}\right) \\
& + \left(\frac{r_0^2}{4\pi}\right)^2 \left[\int \exp\left(-\frac{r_0^2}{4}|\boldsymbol{\alpha}|^2 + i\boldsymbol{\alpha} \cdot \mathbf{y} + \frac{k_0^2}{4} \int_0^L C\left(\mathbf{x} + \frac{\mathbf{h}}{2} - \boldsymbol{\alpha} \frac{z}{k_0}\right) - C(\mathbf{0}) dz\right) d\boldsymbol{\alpha} \right] \\
& \times \left[\int \exp\left(-\frac{r_0^2}{4}|\boldsymbol{\alpha}|^2 - i\boldsymbol{\alpha} \cdot \mathbf{y} + \frac{k_0^2}{4} \int_0^L C\left(\mathbf{x} - \frac{\mathbf{h}}{2} - \boldsymbol{\alpha} \frac{z}{k_0}\right) - C(\mathbf{0}) dz\right) d\boldsymbol{\alpha} \right] \\
& + \left(\frac{r_0 \rho_0}{4\pi}\right)^2 \int \exp\left(-\frac{r_0^2 + \rho_0^2}{8}(|\boldsymbol{\alpha}|^2 + |\boldsymbol{\beta}|^2) + \frac{r_0^2 - \rho_0^2}{4} \boldsymbol{\alpha} \cdot \boldsymbol{\beta} + i(\boldsymbol{\alpha} - \boldsymbol{\beta}) \cdot \mathbf{y}\right) \\
& \times \exp\left(-\frac{k_0^2 C(\mathbf{0})L}{2} + \frac{k_0^2}{4} \int_0^L C\left(\mathbf{h} - \boldsymbol{\alpha} \frac{z}{k_0}\right) + C\left(\boldsymbol{\beta} \frac{z}{k_0}\right) dz\right) d\boldsymbol{\alpha} d\boldsymbol{\beta}.
\end{aligned} \tag{4.7}$$

As a consequence we can now describe the covariance function of the refocused field at offsets $\mathbf{x} + \mathbf{h}/2$ and $\mathbf{x} - \mathbf{h}/2$ (relatively to the original source location \mathbf{y}/ε) defined by

$$\begin{aligned}
& \text{Cov} \left(\hat{u}_{\text{tr}}^\varepsilon \left(\frac{\mathbf{y}}{\varepsilon} + \mathbf{x} + \frac{\mathbf{h}}{2}; \frac{\mathbf{y}}{\varepsilon} \right), \hat{u}_{\text{tr}}^\varepsilon \left(\frac{\mathbf{y}}{\varepsilon} + \mathbf{x} - \frac{\mathbf{h}}{2}; \frac{\mathbf{y}}{\varepsilon} \right) \right) \\
& = \mathbb{E} \left[\hat{u}_{\text{tr}}^\varepsilon \left(\frac{\mathbf{y}}{\varepsilon} + \mathbf{x} + \frac{\mathbf{h}}{2}; \frac{\mathbf{y}}{\varepsilon} \right) \overline{\hat{u}_{\text{tr}}^\varepsilon \left(\frac{\mathbf{y}}{\varepsilon} + \mathbf{x} - \frac{\mathbf{h}}{2}; \frac{\mathbf{y}}{\varepsilon} \right)} \right] \\
& \quad - \mathbb{E} \left[\hat{u}_{\text{tr}}^\varepsilon \left(\frac{\mathbf{y}}{\varepsilon} + \mathbf{x} + \frac{\mathbf{h}}{2}; \frac{\mathbf{y}}{\varepsilon} \right) \right] \mathbb{E} \left[\overline{\hat{u}_{\text{tr}}^\varepsilon \left(\frac{\mathbf{y}}{\varepsilon} + \mathbf{x} - \frac{\mathbf{h}}{2}; \frac{\mathbf{y}}{\varepsilon} \right)} \right].
\end{aligned}$$

PROPOSITION 4.2. *The covariance function of the refocused field satisfies*

$$\begin{aligned}
 & \text{Cov} \left(\hat{u}_{\text{tr}}^\varepsilon \left(\frac{\mathbf{y}}{\varepsilon} + \mathbf{x} + \frac{\mathbf{h}}{2}; \frac{\mathbf{y}}{\varepsilon} \right), \hat{u}_{\text{tr}}^\varepsilon \left(\frac{\mathbf{y}}{\varepsilon} + \mathbf{x} - \frac{\mathbf{h}}{2}; \frac{\mathbf{y}}{\varepsilon} \right) \right) \\
 & \xrightarrow{\varepsilon \rightarrow 0} \left(\frac{r_0 \rho_0}{4\pi} \right)^2 \iint \exp \left(-\frac{r_0^2 + \rho_0^2}{8} (|\boldsymbol{\alpha}|^2 + |\boldsymbol{\beta}|^2) + \frac{r_0^2 - \rho_0^2}{4} \boldsymbol{\alpha} \cdot \boldsymbol{\beta} + i(\boldsymbol{\alpha} - \boldsymbol{\beta}) \cdot \mathbf{y} \right) \\
 (4.8) \quad & \times \exp \left(-\frac{k_0^2 C(\mathbf{0})L}{2} \right) \left[\exp \left(\frac{k_0^2}{4} \int_0^L C \left(\mathbf{h} - \boldsymbol{\alpha} \frac{z}{k_0} \right) + C \left(\boldsymbol{\beta} \frac{z}{k_0} \right) dz \right) - 1 \right] d\boldsymbol{\alpha} d\boldsymbol{\beta}.
 \end{aligned}$$

Note that the covariance does not depend on the central off-set \mathbf{x} . This means in particular that the variance of the refocused field is constant in the neighborhood of the original source location.

The refocused wave $\mathbf{x} \rightarrow \hat{u}_{\text{tr}}^\varepsilon(\mathbf{y}/\varepsilon + \mathbf{x}; \mathbf{y}/\varepsilon)$ therefore consists of a main peak centered at $\mathbf{x} = \mathbf{0}$, of the form (4.2), with peak intensity (square difference between the maximal amplitude and the background amplitude)

$$\begin{aligned}
 \mathcal{I}_{\text{p},\mathbf{y}} &= |\mathcal{U}_{\text{b},\mathbf{y}} - \mathcal{U}_{\text{p},\mathbf{y}}|^2 \\
 &= \left(\frac{r_0^2}{4\pi} \right)^2 \left| \int \exp \left(i\boldsymbol{\xi} \cdot \mathbf{y} - \frac{r_0^2 |\boldsymbol{\xi}|^2}{4} \right) \right. \\
 (4.9) \quad & \times \exp \left(-\frac{k_0^2 C(\mathbf{0})L}{4} \right) \left[\exp \left(\frac{k_0^2}{4} \int_0^L C \left(\boldsymbol{\xi} \frac{z}{k_0} \right) dz \right) - 1 \right] d\boldsymbol{\xi} \left. \right|^2
 \end{aligned}$$

over a zero-mean fluctuating background with intensity

$$\begin{aligned}
 \mathcal{I}_{\text{b},\mathbf{y}} &= \lim_{\varepsilon \rightarrow 0} \text{Var} \left(\hat{u}_{\text{tr}}^\varepsilon \left(\frac{\mathbf{y}}{\varepsilon} + \mathbf{x}; \frac{\mathbf{y}}{\varepsilon} \right) \right) = \lim_{\varepsilon \rightarrow 0} \mathbb{E} \left[\left| \hat{u}_{\text{tr}}^\varepsilon \left(\frac{\mathbf{y}}{\varepsilon} + \mathbf{x}; \frac{\mathbf{y}}{\varepsilon} \right) \right|^2 \right] - \left| \mathbb{E} \left[\hat{u}_{\text{tr}}^\varepsilon \left(\frac{\mathbf{y}}{\varepsilon} + \mathbf{x}; \frac{\mathbf{y}}{\varepsilon} \right) \right] \right|^2 \\
 &= \left(\frac{r_0 \rho_0}{4\pi} \right)^2 \iint \exp \left(-\frac{r_0^2 + \rho_0^2}{8} (|\boldsymbol{\alpha}|^2 + |\boldsymbol{\beta}|^2) + \frac{r_0^2 - \rho_0^2}{4} \boldsymbol{\alpha} \cdot \boldsymbol{\beta} + i(\boldsymbol{\alpha} - \boldsymbol{\beta}) \cdot \mathbf{y} \right) \\
 (4.10) \quad & \times \exp \left(-\frac{k_0^2 C(\mathbf{0})L}{2} \right) \left[\exp \left(\frac{k_0^2}{4} \int_0^L C \left(\boldsymbol{\alpha} \frac{z}{k_0} \right) + C \left(\boldsymbol{\beta} \frac{z}{k_0} \right) dz \right) - 1 \right] d\boldsymbol{\alpha} d\boldsymbol{\beta}.
 \end{aligned}$$

Let us assume that the covariance function C is isotropic and at least twice differentiable at zero and write it in the form

$$(4.11) \quad C(\mathbf{x}) = \sigma^2 l_c \tilde{C} \left(\frac{|\mathbf{x}|}{l_c} \right)$$

with $\tilde{C}(0) = 1$, $\tilde{C}'(0) = 0$, and $\tilde{C}''(0) = -1$. In this framework $C(\mathbf{0}) = \sigma^2 l_c$ and the correlation radius of the medium is l_c . When the original source is at $\mathbf{y} = \mathbf{0}$, then the peak intensity is

$$\begin{aligned}
 \mathcal{I}_{\text{p},\mathbf{0}} &= \exp \left(-\frac{\sigma^2 k_0^2 l_c L}{2} \right) \left| \int_0^\infty a \exp \left(-\frac{a^2}{2} \right) \right. \\
 (4.12) \quad & \times \left[\exp \left(\frac{\sigma^2 k_0^2 l_c L}{4} \int_0^1 \tilde{C} \left(a \frac{\sqrt{2}L}{k_0 l_c r_0} s \right) ds \right) - 1 \right] da \left. \right|^2,
 \end{aligned}$$

and the background intensity is

$$(4.13) \quad \begin{aligned} \mathcal{I}_{b,\mathbf{0}} &= \left(\frac{2r_0\rho_0}{r_0^2 + \rho_0^2} \right)^2 \exp\left(-\frac{\sigma^2 k_0^2 l_c L}{2}\right) \int_0^\infty \int_0^\infty ab \exp\left(-\frac{a^2+b^2}{2}\right) I_0\left(\frac{r_0^2 - \rho_0^2}{r_0^2 + \rho_0^2} ab\right) \\ &\times \left[\exp\left(\frac{\sigma^2 k_0^2 l_c L}{4} \int_0^1 \tilde{C}\left(a \frac{2L}{k_0 l_c \sqrt{r_0^2 + \rho_0^2}} s\right) + \tilde{C}\left(b \frac{2L}{k_0 l_c \sqrt{r_0^2 + \rho_0^2}} s\right) ds\right) - 1 \right] dadb, \end{aligned}$$

where I_0 is the modified Bessel function of the first kind and order zero. As a consequence we can now describe the SNR of the refocused field.

PROPOSITION 4.3. *If the covariance function C is of the form (4.11), then the contrast or signal-to-noise ratio of the refocused field defined by*

$$(4.14) \quad \text{SNR}_{\text{tr}} = \lim_{\varepsilon \rightarrow 0} \frac{|\mathbb{E}[\hat{u}_{\text{tr}}^\varepsilon(\mathbf{0}; \mathbf{0})] - \lim_{|\mathbf{x}'| \rightarrow \infty} \mathbb{E}[\hat{u}_{\text{tr}}^\varepsilon(\mathbf{x}'; \mathbf{0})]|^2}{\text{Var}(\hat{u}_{\text{tr}}^\varepsilon(\mathbf{x}; \mathbf{0}))}$$

does not depend on \mathbf{x} and it is equal to

$$(4.15) \quad \text{SNR}_{\text{tr}} = \frac{\mathcal{I}_{p,\mathbf{0}}}{\mathcal{I}_{b,\mathbf{0}}},$$

where $\mathcal{I}_{p,\mathbf{0}}$ is given by (4.12) and $\mathcal{I}_{b,\mathbf{0}}$ is given by (4.13).

In order to make the discussion more explicit, we assume in the following that scattering is strong in the sense that the propagation distance is larger than the scattering mean free path $\sigma^2 k_0^2 l_c L \gg 1$. The scattering mean free path $L_{\text{sca}} = 4/(\sigma^2 k_0^2 l_c)$ determines the exponential decay rate of the mean amplitude of a wave propagating through the random medium, which decays as $\exp(-k_0^2 C(\mathbf{0})L/8) = \exp(-\sigma^2 k_0^2 l_c L/8) = \exp(-L/(2L_{\text{sca}}))$ with $L_{\text{sca}} = 4/(\sigma^2 k_0^2 l_c)$, as can be seen from the Itô's form (2.8). Using (4.2) with $\mathbf{y} = \mathbf{0}$, we then find that the main peak is a Gaussian peak centered at $\mathbf{0}$,

$$(4.16) \quad \mathbb{E}[\hat{u}_{\text{tr}}^\varepsilon(\mathbf{x}; \mathbf{0})] \xrightarrow{\varepsilon \rightarrow 0} \frac{1}{1 + \frac{\sigma^2 L^3}{6r_0^2 l_c}} \exp\left(-\frac{1 + \frac{\sigma^2 L^3}{24r_0^2 l_c}}{1 + \frac{\sigma^2 L^3}{6r_0^2 l_c}} \frac{\sigma^2 k_0^2 L}{8l_c} |\mathbf{x}|^2\right),$$

which is independent of ρ_0 . The width of the peak is R_{tr} given by

$$(4.17) \quad R_{\text{tr}}^2 = \frac{4l_c}{\sigma^2 k_0^2 L} \frac{1 + \frac{\sigma^2 L^3}{6r_0^2 l_c}}{1 + \frac{\sigma^2 L^3}{24r_0^2 l_c}},$$

and the peak intensity is

$$(4.18) \quad \mathcal{I}_{p,\mathbf{0}} = \frac{1}{\left(1 + \frac{\sigma^2 L^3}{6r_0^2 l_c}\right)^2}.$$

From (4.10) the background intensity is

$$(4.19) \quad \mathcal{I}_{b,\mathbf{0}} = \frac{1}{\left(1 + \frac{\sigma^2 L^3}{6r_0^2 l_c}\right) \left(1 + \frac{\sigma^2 L^3}{6\rho_0^2 l_c}\right)}.$$

As a result the signal-to-noise ratio is given by

$$(4.20) \quad \text{SNR}_{\text{tr}} = \frac{1 + \frac{\sigma^2 L^3}{6\rho_0^2 l_c}}{1 + \frac{\sigma^2 L^3}{6r_0^2 l_c}},$$

and it depends on ρ_0 .

We may identify three situations (remember we always have $r_0 \geq \rho_0$, and we are mainly interested in the case $r_0 \gg \rho_0$):

$$(4.21) \quad \text{SNR}_{\text{tr}} \approx \begin{cases} 1 & \text{if } \rho_0^2 > \frac{\sigma^2 L^3}{6l_c}, \\ \frac{\sigma^2 L^3}{6\rho_0^2 l_c} & \text{if } \rho_0^2 < \frac{\sigma^2 L^3}{6l_c} < r_0^2, \\ \frac{r_0^2}{\rho_0^2} & \text{if } r_0^2 < \frac{\sigma^2 L^3}{6l_c}. \end{cases}$$

This shows that stability increases when the number of elements of the TRM increases, or equivalently when the radius ρ_0 decreases. As a function of r_0 the signal-to-noise ratio is maximal when $r_0^2 < \sigma^2 L^3 / (6l_c)$, and then it is given by the number of elements of the TRM r_0^2 / ρ_0^2 . We can explain the physical origin of the condition $r_0^2 < \sigma^2 L^3 / (6l_c)$ as follows. The field generated by the original source at the target point $(\mathbf{0}, L)$, transmitted through the medium, and recorded by the TRM, has the form of a diffuse beam with radius of the order of $\sigma^2 L^3 / l_c$ [9]. If the radius of the TRM is larger, then the elements of the TRM outside the support of the diffuse beam do not record anything and cannot participate in the time-reversal process. They are not used at all, which is why the SNR cannot reach its maximal value given by the number of elements of the TRM r_0^2 / ρ_0^2 .

5. Focusing at a prescribed target point. It was noticed in the experiments that wave focusing could be achieved with the optimized phases of the SLM in the neighborhood of the target point and not only on the target point [15, 20]. In the time-reversal context, this amounts to saying that, for a given original point source at (\mathbf{y}, L) , it is possible to manipulate the field emitted by the TRM to focus on a point prescribed by the user near (\mathbf{y}, L) . In this section we introduce and discuss this manipulation and we explain and quantify the refocusing property on a prescribed point (see Figure 3).

In order to shift the focal spot of the refocused wave the idea is to impose an additional linear phase at the TRM, so that the field in the plane $z = L$ is instead of (2.2):

$$(5.1) \quad \hat{u}_{\text{tr}}^{\mathbf{b}}(\mathbf{x}; \mathbf{y}) = \int \exp\left(-\frac{|\mathbf{x}_m|^2}{R_m^2} + \frac{i\mathbf{b} \cdot \mathbf{x}_m}{R_m^2}\right) \hat{u}_{\text{em}}(\mathbf{x}, \mathbf{x}_m) \overline{\hat{u}_{\text{rec}}(\mathbf{x}_m; \mathbf{y})} d\mathbf{x}_m,$$

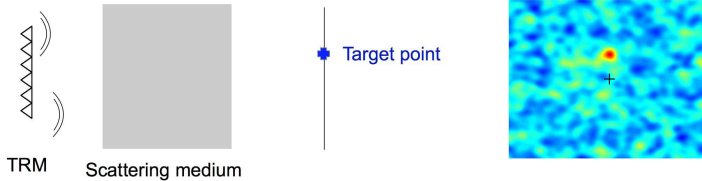


FIG. 3. Focusing on a prescribed point in the neighborhood of the original source location. The TRM emits the complex-conjugated recorded field with an additional linear phase. The right picture shows the transmitted field in the target plane. The cross in the right picture is the original source location. The prescribed (target) point is above the source point. One can see that the transmitted field in the target plane has a focal spot at the prescribed point.

where \hat{u}_{rec} has been obtained with a point source at (\mathbf{y}, L) and is given by (2.1). The vector \mathbf{b} determines the linear phase and we will see below how to choose it to focus on a prescribed point. The time-reversed field can therefore be expressed as

$$(5.2) \quad \hat{u}_{\text{tr}}^{\mathbf{b}}(\mathbf{x}; \mathbf{y}) = 4k_0^2 C_0 \exp\left(-\frac{\rho_0^2}{4r_0^2(r_0^2 - \rho_0^2)}|\mathbf{b}|^2\right) \iint \exp\left(-\frac{|\mathbf{x}'|^2}{r_0^2} - \frac{|\mathbf{y}'|^2}{4\rho_0^2} + i\frac{\mathbf{b} \cdot \mathbf{x}'}{r_0^2}\right) \times \hat{G}\left(L, \mathbf{x}' + \frac{\mathbf{y}'}{2}, \mathbf{x}\right) \overline{\hat{G}\left(L, \mathbf{x}' - \frac{\mathbf{y}'}{2}, \mathbf{y}\right)} d\mathbf{x}' d\mathbf{y}'$$

with C_0 and r_0 defined by (2.5). We will take $C_0 = 1$ as in the previous sections.

We proceed as in the previous section. We consider the scintillation regime $C \rightarrow \varepsilon C$, $r_0 \rightarrow r_0/\varepsilon$, $\rho_0 \rightarrow \rho_0/\varepsilon$, $\mathbf{y} \rightarrow \mathbf{y}/\varepsilon$, $L \rightarrow L/\varepsilon$, $\mathbf{b} \rightarrow \mathbf{b}/\varepsilon$. The mean refocused wave at offset \mathbf{x} (relatively to the original source location \mathbf{y}/ε) is then of the form

$$(5.3) \quad \mathbb{E}\left[\hat{u}_{\text{tr}}^{\mathbf{b},\varepsilon}\left(\frac{\mathbf{y}}{\varepsilon} + \mathbf{x}; \frac{\mathbf{y}}{\varepsilon}\right)\right] \xrightarrow{\varepsilon \rightarrow 0} \frac{r_0^2}{4\pi} \exp\left(-\frac{\rho_0^2}{4r_0^2(r_0^2 - \rho_0^2)}|\mathbf{b}|^2\right) \int \exp\left(i\boldsymbol{\xi} \cdot \mathbf{y} - \frac{r_0^2}{4}\left|\boldsymbol{\xi} - \frac{\mathbf{b}}{r_0^2}\right|^2\right) \times \exp\left(\frac{k_0^2}{4} \int_0^L C\left(\mathbf{x} - \boldsymbol{\xi} \frac{z}{k_0}\right) - C(\mathbf{0}) dz\right) d\boldsymbol{\xi}.$$

The variance function of the refocused field at offset \mathbf{x} satisfies

$$(5.4) \quad \text{Var}\left(\hat{u}_{\text{tr}}^{\mathbf{b},\varepsilon}\left(\frac{\mathbf{y}}{\varepsilon} + \mathbf{x}; \frac{\mathbf{y}}{\varepsilon}\right)\right) = \mathbb{E}\left[\left|\hat{u}_{\text{tr}}^{\mathbf{b},\varepsilon}\left(\frac{\mathbf{y}}{\varepsilon} + \mathbf{x}; \frac{\mathbf{y}}{\varepsilon}\right)\right|^2\right] - \left|\mathbb{E}\left[\hat{u}_{\text{tr}}^{\mathbf{b},\varepsilon}\left(\frac{\mathbf{y}}{\varepsilon} + \mathbf{x}; \frac{\mathbf{y}}{\varepsilon}\right)\right]\right|^2 \xrightarrow{\varepsilon \rightarrow 0} \left(\frac{r_0\rho_0}{4\pi}\right)^2 \exp\left(-\frac{\rho_0^2}{2r_0^2(r_0^2 - \rho_0^2)}|\mathbf{b}|^2 - \frac{k_0^2 C(\mathbf{0})L}{2}\right) \times \iint \exp\left(-\frac{r_0^2 + \rho_0^2}{8}(|\boldsymbol{\alpha}|^2 + |\boldsymbol{\beta}|^2) + \frac{r_0^2 - \rho_0^2}{4}\boldsymbol{\alpha} \cdot \boldsymbol{\beta} + i(\boldsymbol{\alpha} - \boldsymbol{\beta}) \cdot \mathbf{y}\right) \times \left[\exp\left(\frac{k_0^2}{4} \int_0^L C(\boldsymbol{\alpha} \frac{z}{k_0}) + C(\boldsymbol{\beta} \frac{z}{k_0}) dz\right) - 1\right] d\boldsymbol{\alpha} d\boldsymbol{\beta}.$$

Assume that the covariance function $C(\mathbf{x})$ has the form (4.11). When scattering is strong in the sense that the propagation distance is larger than the scattering mean free path $\sigma^2 k_0^2 l_c L \gg 1$, the main peak is of the form of a damped and shifted Gaussian peak

$$(5.5) \quad \mathbb{E}\left[\hat{u}_{\text{tr}}^{\mathbf{b},\varepsilon}(\mathbf{x}; \mathbf{0})\right] \xrightarrow{\varepsilon \rightarrow 0} \frac{1}{1 + \frac{\sigma^2 L^3}{6r_0^2 l_c}} \exp\left(-\frac{|\mathbf{b}|^2}{4r_0^2} \left(\frac{\frac{\sigma^2 L^3}{24l_c}}{r_0^2 + \frac{\sigma^2 L^3}{24l_c}} + \frac{\rho_0^2}{r_0^2 - \rho_0^2}\right)\right) \exp\left(-\frac{|\mathbf{x} - \mathbf{x}^{\mathbf{b}}|^2}{2R_{\text{tr}}^2}\right),$$

whose center is at

$$(5.6) \quad \mathbf{x}^{\mathbf{b}} = \alpha_L \mathbf{b}, \quad \alpha_L = \frac{L}{2k_0 r_0^2 \left(1 + \frac{\sigma^2 L^3}{24r_0^2 l_c}\right)},$$

and the width R_{tr} is given by (4.17). This shows that the linear phase \mathbf{b} in (5.1) generates a shift in the focal spot that is deterministic, proportional to the linear phase, and fully predictable. If $\frac{\sigma^2 L^3}{24l_c} \ll r_0^2$, then $\alpha_L = L/(2k_0 r_0^2)$ and therefore the linear phase that one needs to impose to get focusing on a prescribed point is easy to compute. If $\frac{\sigma^2 L^3}{24l_c} \geq r_0^2$, then α_L is given by (5.6) and therefore one should know the

statistics of the random medium to get focusing on a prescribed point. More exactly, if one wants to focus at the target point (\mathbf{x}_t, L) , then one imposes the phase

$$(5.7) \quad \mathbf{b}_t = \frac{1}{\alpha_L} \mathbf{x}_t.$$

The shift that can be imposed is in fact limited by the SNR. Indeed, the peak intensity $\mathcal{I}_{p,0}^b$ is damped when the shift becomes large,

$$(5.8) \quad \begin{aligned} \mathcal{I}_{p,0}^b &= \lim_{\varepsilon \rightarrow 0} \left| \mathbb{E}[\hat{u}_{\text{tr}}^{\mathbf{b},\varepsilon}(\mathbf{x}^b; \mathbf{0})] \right|^2 \\ &= \frac{1}{\left(1 + \frac{\sigma^2 L^3}{6r_0^2 l_c}\right)^2} \exp\left(-\frac{|\mathbf{b}|^2}{2r_0^2} \left(\frac{\sigma^2 L^3}{24l_c} + \frac{\rho_0^2}{r_0^2 - \rho_0^2}\right)\right), \end{aligned}$$

while the mean intensity of the background fluctuations is

$$(5.9) \quad \begin{aligned} \mathcal{I}_{b,0}^b &= \lim_{\varepsilon \rightarrow 0} \text{Var}\left(\hat{u}_{\text{tr}}^{\mathbf{b},\varepsilon}(\mathbf{x}; \mathbf{0})\right) = \lim_{\varepsilon \rightarrow 0} \mathbb{E}\left[|\hat{u}_{\text{tr}}^{\mathbf{b},\varepsilon}(\mathbf{x}; \mathbf{0})|^2\right] - \left|\mathbb{E}[\hat{u}_{\text{tr}}^{\mathbf{b},\varepsilon}(\mathbf{x}; \mathbf{0})]\right|^2 \\ &= \frac{1}{\left(1 + \frac{\sigma^2 L^3}{6r_0^2 l_c}\right) \left(1 + \frac{\sigma^2 L^3}{6\rho_0^2 l_c}\right)} \exp\left(-\frac{|\mathbf{b}|^2}{2r_0^2} \frac{\rho_0^2}{r_0^2 - \rho_0^2}\right), \end{aligned}$$

which is independent of \mathbf{x} . As a result the signal-to-noise ratio of the shifted peak at \mathbf{x}^b is

$$(5.10) \quad \begin{aligned} \text{SNR}_{\text{tr}}^b &= \frac{\mathcal{I}_{p,0}^b}{\mathcal{I}_{b,0}^b} = \frac{1 + \frac{\sigma^2 L^3}{6\rho_0^2 l_c}}{1 + \frac{\sigma^2 L^3}{6r_0^2 l_c}} \exp\left(-\frac{|\mathbf{b}|^2}{2r_0^2} \frac{\sigma^2 L^3}{r_0^2 + \frac{\sigma^2 L^3}{24l_c}}\right) \\ &= \text{SNR}_{\text{tr}} \exp\left(-\frac{|\mathbf{b}|^2}{2r_0^2} \frac{\sigma^2 L^3}{r_0^2 + \frac{\sigma^2 L^3}{24l_c}}\right), \end{aligned}$$

where SNR_{tr} is the signal-to-noise ratio (4.20) of the time-reversed refocused peak. To observe refocusing, the SNR_{tr}^b of the shifted peak should be larger than one, and this means that one should limit the shift to $|\mathbf{b}| \leq b_{\max}$ with

$$(5.11) \quad b_{\max}^2 = 2r_0^2 \left(1 + \frac{24r_0^2 l_c}{\sigma^2 L^3}\right) \ln \frac{1 + \frac{\sigma^2 L^3}{6\rho_0^2 l_c}}{1 + \frac{\sigma^2 L^3}{6r_0^2 l_c}}.$$

This result with (5.6) shows that it is possible to focus in a region around the original source point whose radius $R_{\max} = \alpha_L b_{\max}$ is given by

$$(5.12) \quad \begin{aligned} R_{\max}^2 &= \frac{12l_c}{\sigma^2 k_0^2 L \left(1 + \frac{\sigma^2 L^3}{24r_0^2 l_c}\right)} \ln \frac{1 + \frac{\sigma^2 L^3}{6\rho_0^2 l_c}}{1 + \frac{\sigma^2 L^3}{6r_0^2 l_c}} \\ &= \frac{3R_{\text{tr}}^2}{1 + \frac{\sigma^2 L^3}{6r_0^2 l_c}} \ln \text{SNR}_{\text{tr}}. \end{aligned}$$

Thus, the focusing region increases as the logarithm of the SNR_{tr} (4.20).

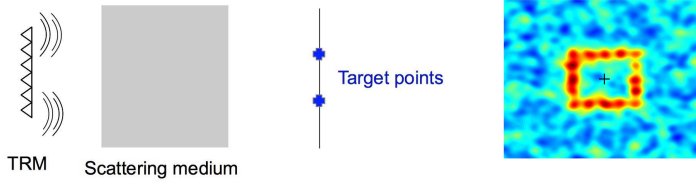


FIG. 4. Transmission of an image, here a square that consists of a set of 16 target points. The TRM emits the superposition of 16 fields. Each emitted field is the complex-conjugated recorded field with an appropriate additional linear phase that creates a focal spot at one of the 16 target points in the target plane. The right picture shows the transmitted field in the target plane. The cross in the right picture is the original source location. The transmitted image (the square) can be clearly seen in the transmitted field plotted in the right picture.

6. Imaging through a complex medium. The experimental observation that wave focusing can be achieved with the optimized phases of the SLM in the neighborhood of the target point and not only on the target point is essential because it shows that an image can be transmitted once the phases of the SLM have been optimized for a target point. This was achieved experimentally in [15, 20], for instance. In this section we quantify the resolution and stability properties of the transmitted image. In the previous section we discussed focusing to one prescribed point in the neighborhood of the original source point as in Figure 3. This was accomplished by adding a linear phase in the process of time reversal and reemission. The size of the neighborhood to which we can stably transmit is limited as described by (5.12). In this section we generalize this to transmission of images. One may think of this as transmission of a set of pixels forming an image and where each pixel can be transmitted as explained above. We illustrate this in Figure 4, where a set of points are transmitted to form an image in the target plane. The figure shows clearly how we can transmit an image in the form of a square, clearly visible on top of the background speckle. Note that each point in the target plane can be associated with a particular linear phase in the transmission. The procedure of forming the field that the TRM should emit in order to transmit a general image can then conveniently be formulated in terms of the Fourier transform of the image and we discuss this next.

In the time-reversal context, let $\psi(\mathbf{x})$ be a real-valued function that is the image to be transmitted. It could be a discrete image, i.e., ψ is a sum of Dirac distributions, or a continuous one, i.e., ψ is a bounded and compactly supported function. Let us denote by $\hat{\psi}$ the Fourier transform of ψ :

$$\hat{\psi}(\boldsymbol{\xi}) = \int \psi(\mathbf{x}) \exp(-i\mathbf{x} \cdot \boldsymbol{\xi}) d\mathbf{x}.$$

Let us emit the function $\overline{\hat{\psi}(\mathbf{x}_m/R_m^2)} \hat{u}_{\text{rec}}(\mathbf{x}_m; \mathbf{0})$ from the TRM and consider the refocused wave

$$(6.1) \quad \hat{u}_{\text{tr}}^\psi(\mathbf{x}; \mathbf{0}) = \int \hat{u}_{\text{em}}(\mathbf{x}, \mathbf{x}_m) \exp\left(-\frac{|\mathbf{x}_m|^2}{R_m^2}\right) \overline{\hat{\psi}\left(\frac{\mathbf{x}_m}{R_m^2}\right)} \hat{u}_{\text{rec}}(\mathbf{x}_m; \mathbf{0}) d\mathbf{x}_m,$$

where $\hat{u}_{\text{rec}}(\mathbf{x}_m; \mathbf{0})$ has been obtained with a point source at $(\mathbf{0}, L)$. By noting that the refocused wave can be expressed as

$$(6.2) \quad \hat{u}_{\text{tr}}^\psi(\mathbf{x}; \mathbf{0}) = \int \psi(\mathbf{b}) \hat{u}_{\text{tr}}^{\mathbf{b}}(\mathbf{x}; \mathbf{0}) d\mathbf{b},$$

with \hat{u}_{tr}^b defined by (5.1), the analysis of the image formation in the target plane $z = L$ follows from the results obtained in the previous section.

In the scintillation regime, $C \rightarrow \varepsilon C$, $r_0 \rightarrow r_0/\varepsilon$, $\rho_0 \rightarrow \rho_0/\varepsilon$, $L \rightarrow L/\varepsilon$, $\psi(\mathbf{x}) \rightarrow \varepsilon^2 \psi(\varepsilon \mathbf{x})$, the refocused wave can be expressed as

$$(6.3) \quad \hat{u}_{\text{tr}}^{\psi, \varepsilon}(\mathbf{x}; \mathbf{0}) = \int \psi(\mathbf{b}) \hat{u}_{\text{tr}}^{b, \varepsilon}(\mathbf{x}; \mathbf{0}) d\mathbf{b}.$$

When scattering is strong $\sigma^2 k_0^2 l_c L \gg 1$ its expectation satisfies

$$(6.4) \quad \begin{aligned} \mathbb{E}[\hat{u}_{\text{tr}}^{\psi, \varepsilon}(\mathbf{x}; \mathbf{0})] &\xrightarrow{\varepsilon \rightarrow 0} \frac{1}{1 + \frac{\sigma^2 L^3}{6r_0^2 l_c}} \int \frac{1}{\alpha_L^2} \psi\left(\frac{\mathbf{x}'}{\alpha_L}\right) \exp\left(-\frac{|\mathbf{x} - \mathbf{x}'|^2}{2R_{\text{tr}}^2}\right) \\ &\times \exp\left(-\frac{|\mathbf{x}'|^2}{4r_0^2 \alpha_L^2} \left(\frac{\sigma^2 L^3}{24l_c} + \frac{\rho_0^2}{r_0^2 - \rho_0^2}\right)\right) d\mathbf{x}', \end{aligned}$$

and its fluctuations are relatively smaller than its expectation provided the support of ψ is within the disk with radius b_{max} defined by (5.11). This gives an image of ψ up to a dilatation by the factor α_L which is supported within the disk with radius $R_{\text{max}} = \alpha_L b_{\text{max}}$. The expression (6.4) also shows that the dilated version $\psi(\cdot/\alpha_L)$ is imaged up to a radial attenuation and up to a convolution with a Gaussian kernel with radius R_{tr} . From (5.12) we have

$$R_{\text{max}}^2 = \frac{3R_{\text{tr}}^2}{1 + \frac{\sigma^2 L^3}{6r_0^2 l_c}} \ln \frac{1 + \frac{\sigma^2 L^3}{6\rho_0^2 l_c}}{1 + \frac{\sigma^2 L^3}{6r_0^2 l_c}}.$$

The transmitted image is acceptable if $R_{\text{tr}} < R_{\text{max}}$; otherwise the smoothing by the Gaussian kernel with radius R_{tr} in (6.4) blurs the image. Therefore a favorable situation is when the radius of the TRM is large so that $\sigma^2 L^3/(6r_0^2 l_c) \lesssim 1$ and when it has a large number of elements so that $\sigma^2 L^3/(6\rho_0^2 l_c) \gg 1$. In this situation $R_{\text{max}} \gg R_{\text{tr}}$ and the image is not significantly blurred, although the propagation distance through the complex medium is much larger than the scattering mean free path. This shows that image transmission can be achieved through a strongly scattering medium by the SLM or time-reversal technique.

7. Conclusion. Time reversal allows for wave refocusing through a complex medium. This is true even when the elements of the TRM are larger than the correlation radius of the field that it records and that comes from a point source at a target point on the other side of the medium. When refocusing on the target point, the profile of the mean focal spot depends on the diameter of the TRM but it does not depend on the number of elements of the TRM (provided it is large enough). However the signal-to-noise ratio strongly depends on the number of elements of the TRM. Moreover, we have shown that when the field emitted by a point source in the target plane has been recorded by the TRM, then it is also possible to focus a wave on a target point in the neighborhood of the original point source. It is even possible to transmit an image. The transmission of an image is possible provided the radius of the TRM is large enough and contains a large number of elements. All these results are quantified in this paper in the white-noise paraxial regime, which is a regime relevant for laser beam propagation in scattering media and in turbulent atmosphere in particular.

Appendix A. Scintillation regime in the white-noise paraxial model.

The Itô–Schrödinger model in (2.6), which is also referred to as the white-noise

paraxial model, is widely used in the physical literature. It simplifies the full wave equation by replacing it with an initial value problem in the half-space $z > 0$ with the field at $z = 0$ given. It was studied mathematically in [3]. The proof of its derivation from the three-dimensional wave equation in a randomly scattering medium is given in [9]. Note that in the context of laser beam propagation the propagation phenomenon is often modeled in terms of the scalar wave equation, and moreover, in terms of the paraxial equation, and this is the context that we want to consider here [1]. Polarization effects may be relevant in certain situations, but here we do not consider such effects.

The white-noise paraxial model (2.6) can be obtained from the three-dimensional scalar wave equation by a separation of scales technique in which the three-dimensional fluctuations of the index of refraction $n(z, \mathbf{x})$ are described by a zero-mean stationary random process $\nu(z, \mathbf{x})$ with mixing properties: $n^2(z, \mathbf{x}) = 1 + \nu(z, \mathbf{x})$. The covariance function $C(\mathbf{x})$ in (2.7) is then given in terms of the two-point statistics of the random process ν by

$$(A.1) \quad C(\mathbf{x}) = \int_{-\infty}^{\infty} \mathbb{E}[\nu(z' + z, \mathbf{x}' + \mathbf{x})\nu(z', \mathbf{x}')] dz.$$

The model (2.6) is valid when the wavelength is smaller than the radius of the beam and the correlation radius of the medium, which are themselves smaller than the typical propagation distance. The moments of the field then satisfy closed-form transport equations. If, additionally, the correlation radius of the medium is smaller than the radius of the beam, then the situation corresponds to the scintillation regime and the transport equation for the fourth-order moment can be solved as was shown in [12] and as we state in section 3.

Acknowledgment. We thank Dr. Arje Nachman for suggesting the above problem.

REFERENCES

- [1] L. C. ANDREWS AND R. L. PHILIPPS, *Laser Beam Propagation Through Random Media*, SPIE Press, Bellingham, WA, 2005.
- [2] P. BLOMGREN, G. PAPANICOLAOU, AND H. ZHAO, *Super-resolution in time-reversal acoustics*, J. Acoust. Soc. Am., 111 (2002), pp. 230–248.
- [3] D. DAWSON AND G. PAPANICOLAOU, *A random wave process*, Appl. Math. Optim., 12 (1984), pp. 97–114.
- [4] S. FENG, C. KANE, P. A. LEE, AND A. D. STONE, *Correlations and fluctuations of coherent wave transmission through disordered media*, Phys. Rev. Lett., 61 (1988), pp. 834–837.
- [5] J.-P. FOUQUE, J. GARNIER, G. PAPANICOLAOU, AND K. SØLNA, *Wave Propagation and Time Reversal in Randomly Layered Media*, Springer, New York, 2007.
- [6] J.-P. FOUQUE, G. PAPANICOLAOU, AND Y. SAMUELIDES, *Forward and Markov approximation: The strong-intensity-fluctuations regime revisited*, Waves Random Media, 8 (1998), pp. 303–314.
- [7] I. FREUND, M. ROSENBLUH, AND S. FENG, *Memory effects in propagation of optical waves through disordered media*, Phys. Rev. Lett., 61 (1988), pp. 2328–2331.
- [8] J. GARNIER AND K. SØLNA, *Random backscattering in the parabolic scaling*, J. Stat. Phys., 131 (2008), pp. 445–486.
- [9] J. GARNIER AND K. SØLNA, *Coupled paraxial wave equations in random media in the white-noise regime*, Ann. Appl. Probab., 19 (2009), pp. 318–346.
- [10] J. GARNIER AND K. SØLNA, *Scaling limits for wave pulse transmission and reflection operators*, Wave Motion, 46 (2009), pp. 122–143.
- [11] J. GARNIER AND K. SØLNA, *Scintillation in the white-noise paraxial regime*, Comm. Partial Differential Equations, 39 (2014), pp. 626–650.

- [12] J. GARNIER AND K. SØLNA, *Fourth-moment analysis for beam propagation in the white-noise paraxial regime*, Arch. Ration. Mech. Anal., 220 (2016), pp. 37–81.
- [13] J. W. GOODMAN, *Statistical Optics*, Wiley, New York, 2000.
- [14] A. ISHIMARU, *Wave Propagation and Scattering in Random Media*, Academic Press, San Diego, CA, 1978.
- [15] O. KATZ, E. SMALL, AND Y. SILBERBERG, *Looking around corners and through thin turbid layers in real time with scattered incoherent light*, Nature Photon., 6 (2012), pp. 549–553.
- [16] G. LEROSEY, J. DE ROSNY, A. TOURIN, AND M. FINK, *Focusing beyond the diffraction limit with far-field time reversal*, Science, 315 (2007), pp. 1120–1122.
- [17] A. P. MOSK, A. LAGENDIJK, G. LEROSEY, AND M. FINK, *Controlling waves in space and time for imaging and focusing in complex media*, Nature Photon., 6 (2012), pp. 283–292.
- [18] G. PAPANICOLAOU, L. RYZHIK, AND K. SØLNA, *Statistical stability in time reversal*, SIAM J. Appl. Math., 64 (2004), pp. 1133–1155.
- [19] S. M. POPOFF, A. GOETSCHY, S. F. LIEW, A. D. STONE, AND H. CAO, *Coherent control of total transmission of light through disordered media*, Phys. Rev. Lett., 112 (2014), 133903.
- [20] S. POPOFF, G. LEROSEY, M. FINK, A. C. BOCCARA, AND S. GIGAN, *Image transmission through an opaque material*, Nature Commun., 1 (2010), pp. 1–5.
- [21] J. W. STROHBEHN, ED., *Laser Beam Propagation in the Atmosphere*, Springer, Berlin, 1978.
- [22] F. TAPPERT, *The parabolic approximation method*, in Wave Propagation and Underwater Acoustics, J. B. Keller and J. S. Papadakis, eds., Springer, Berlin, 1977, pp. 224–287.
- [23] I. M. VELLEKOOP, A. LAGENDIJK, AND A. P. MOSK, *Exploiting disorder for perfect focusing*, Nature Photon., 4 (2010), pp. 320–322.
- [24] I. M. VELLEKOOP AND A. P. MOSK, *Focusing coherent light through opaque strongly scattering media*, Opt. Lett., 32 (2007), pp. 2309–2311.
- [25] I. M. VELLEKOOP AND A. P. MOSK, *Universal optimal transmission of light through disordered materials*, Phys. Rev. Lett., 101 (2008), 120601.